CONF-800551--7

LA-UR 80-1328

**TITLE:** EVALUATION OF NEUTRON CROSS SECTIONS TO 40 MeV for $^{54,56}$Fe

**AUTHOR(S):** E. D. Arthur and P. G. Young

**SUBMITTED TO:** Symposium on Neutron Cross Sections from 10 to 50 MeV

Brookhaven National Laboratory
May 12-14, 1980



los alamos
scientific laboratory
of the University of California
LOS ALAMOS, NEW MEXICO 87545



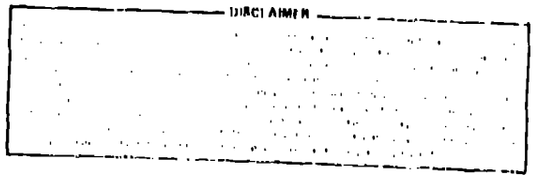


Form No. 836
St. No. 2629
1/75

UNITED STATES
ENERGY RESEARCH AND
DEVELOPMENT ADMINISTRATION
CONTRACT W-7405-ENG. 36

# EVALUATION OF NEUTRON CROSS SECTIONS TO 40 MeV FOR $^{54,56}Fe$*

E. D. Arthur and P. G. Young

Theoretical Division
Los Alamos Scientific Laboratory
University of California
Los Alamos, New Mexico 87545

## ABSTRACT

Cross sections for neutron-induced reactions on $^{54,56}Fe$ were calculated employing several nuclear models--optical, Hauser-Feshbach, preequilibrium, and DWBA--in the energy range between 3 and 40 MeV. As a prelude to the calculations, the necessary input parameters were determined or verified through analysis of a large body of experimental data both for neutron- and proton-induced reactions in this mass and energy region. This technique also led to cross sections in which the simultaneous influence of available data types added to their consistency and reliability. Calculated cross sections as well as neutron and gamma-ray emission spectra were incorporated into an ENDF evaluation suitable for use to 40 MeV.

## INTRODUCTION

As part of an effort to satisfy nuclear data needs for the Fusion Materials Irradiation Test Facility, we performed comprehensive nuclear-model calculations on $^{54,56}Fe$ between 3 and 40 MeV. The results were combined and joined to the existing ENDF/B-V iron evaluation at 3 MeV to produce a new evaluation applicable to 40 MeV that was essentially free of energy balance problems.

Since little experimental data exist for neutron reactions at higher energies (total cross sections are an exception), we relied upon nuclear models--Hauser-Feshbach [1], preequilibrium, optical, and direct reaction--that describe the main mechanisms governing neutron reactions in this mass and energy region. As a first step towards proper use of these models, we determined input parameters

*Work supported by the U.S. Department of Energy.

valid for this calculation. With these parameters we then employed the models in a simultaneous analysis of a large body of available neutron reaction data for iron--cross sections and emission spectra for neutrons, charged particles, and gamma rays. This effort was further aided by the calculation of p + $^{54,56}$Fe reaction data at higher energies using these same parameters. In this approach, the many types of available data produce constraints on the calculated results, providing in the end a set of consistent calculated cross sections as well as input parameters tested under varied and stringent conditions. This approach can allow discrepant or inconsistent data sets to be ascertained since it uses, simultaneously, information from several reaction types available at a given incident energy. Thus, unphysical calculations or parameters resulting from the isolated analysis of a given cross section, data type, or experimental result can be largely avoided.

## PARAMETERS

We determined values for optical model parameters and gamma-ray strength functions, while for level density or preequilibrium parameters we relied on published results that were generally determined through systematic analysis of a substantial amount of experimental data. We did verify (or modify as needed) these parameters where pertinent data were available, but we did not attempt large-scale or systematic adjustments because of the complexities involved.

We devoted an appreciable effort to determination or verification of optical-model and gamma-ray strength function parameters since values were sometimes lacking or were not appropriate to the range of interest in our calculations. Neutron optical parameters received the greatest effort since such parameters must produce realistic formation cross sections for a wide range of energies while providing a reasonable behavior of low-energy transmission coefficients needed in the calculation of reactions such as (n,2n). We determined optical parameters through simultaneous fits to the following neutron data: (1) total cross sections between 2 and 40 MeV, (2) s- and p-wave strength functions and values for the potential scattering radius, (3) elastic scattering angular distributions between 6 and 14 MeV, and (4) reaction cross sections between 5 and 30 MeV. The resulting parameters appear in Table 1, while in Figs. 1 and 2 comparisons are made to the total cross section and elastic-scattering angular distributions. Although reasonable agreement was obtained to the quantities listed above, the predicted nonelastic cross section overestimates new results [2] at 40 MeV that were not available for inclusion in our fit. This overprediction led us to renormalize our calculated Hauser-Feshbach cross sections downward by about 10% in this energy region.

Proton and alpha-particle transmission coefficients were calculated from optical parameters based on published sets [3,4] obtained from data fits in this mass and energy range. We adjusted them to better fit low energy data [(p,n) and (α,n) cross sections] and higher energy information (generally, reaction cross sections) that were available. The modification usually took the form of an energy dependence added to the real and/or imaginary well depths. The modified proton and alpha particle parameters also appear in Table I.

Gamma-ray reactions can be important competitors to particle emission, particularly around thresholds. We chose to normalize gamma-ray transmission coefficients (assumed to be of the Brink-Axel [5] giant dipole resonance form) through determination of gamma-ray strength functions by fits to $^{54,56}$Fe (n,γ) data. This method avoids problems occurring when this normalization is determined directly from the ratio of the average gamma width, $\langle\Gamma_\gamma\rangle$, and spacing $\langle D\rangle$, for s-wave resonances as is often done for each compound nucleus in these types of calculations. Such $\langle\Gamma_\gamma\rangle$ and $\langle D\rangle$ values are not always reliable, particularly where information for compound systems away from the line of stability must be inferred from their systematic behavior. Gamma-ray strength functions should be more reliable since they vary slowly between nearby nuclei. In fact, the strength function determined for $^{55}$Fe and $^{57}$Fe were essentially identical, differing only by about 5%.

Parameters for the Gilbert-Cameron [6] level density model used in these calculations were taken from the values of Cook [7] for the level density constant, a, and the pairing energy, Δ. At lower excitation energies a constant temperature expression was used, the parameters of which we adjusted to agree with the cumulative number of discrete levels while joining smoothly to the Fermi-gas form used at higher energies.

For preequilibrium corrections, we applied the master equations model of Kalbach [8] that employs a matrix element for residual two-body interactions whose absolute square depends upon the excitation energy available per exciton as well as the mass of the compound system [9]. The normalization constant was taken to be 160 MeV$^3$, which is about 20% higher than the value recommended by Kalbach.

Since the preequilibrium and Hauser-Feshbach models do not adequately describe the excitation of collective states in $^{54,56}$Fe through neutron inelastic scattering, we performed DWBA calculations for 24 such states. We used deformation parameters, $\beta_\ell$, determined by Mani [10] from 40 MeV inelastic proton scattering on $^{54,56}$Fe along with the neutron optical parameters appearing in Table I.

## RESULTS AND COMPARISONS TO DATA

Calculations were performed using three nuclear-model codes--(1) DWUCK [11] for DWBA calculations, (2) COMNUC [12] for low energy Hauser-Feshbach calculations with width-fluctuation corrections, and (3) GNASH [13] for higher energy Hauser-Feshbach calculations where preequilibrium corrections were necessary and complex decay chains were followed. In the next few paragraphs, we will compare a portion of the 26 reaction types calculated to experimental data, showing in many cases cross-section values up to 40 MeV.

With the use of evaluated data for shielding and other neutronics purposes, a realistic representation of neutron-emission cross sections, spectra, and angular distributions is of particular importance. Several cross-section types provide the opportunity to evaluate and verify the neutron (and other) parameters used in the calculations as well as indicate features of the data that should be a part of the evaluation if accurate representations are desired. Figure 3 compares the calculated neutron emission spectrum (after incorporation of an appropriate resolution function) to data of Kammerdiener [14]. The lower end of the spectrum consists of evaporation neutrons [mostly from (n,2n) processes] while the middle and upper portions contain preequilibrium neutrons. At the upper part of the spectrum, contributions from discrete levels excited by direct-reaction inelastic scattering are evident both in the data and calculations.

At higher incident energies such emitted neutrons generally become more forward-peaked--not only those resulting from inelastic scattering from discrete levels but also those appearing in the middle and upper continuum regions of the spectrum. Such energy-angle correlations must therefore be incorporated into the evaluated data. Figure 4 compares the DWBA calculated angular distribution to data [15,16] for inelastic scattering from the first excited state of $^{56}$Fe by 14.1 MeV neutrons. The agreement indicates the applicability of both the neutron-optical parameters and the $\beta_2$ value used as obtained from proton scattering results.

To represent angular distributions of continuum neutrons, we used the phenomological expressions recently determined by Kalbach and Mann [17] from fits to particle-induced reaction data. These expressions rely on information concerning the cross-section fraction resulting from multistep direct and multistep compound processes. We approximated these through use of total preequilibrium and evaporation fractions, respectively. The double-differential cross sections thereby obtained at 14 MeV agree reasonably well with the Hermsdorf angular distribution data [18] measured for natural iron.

Neutron inelastic scattering and emission results on iron are complemented by (n,2n) data measured using large liquid scintilla-

tor tanks. The comparison to such data [19,20] as shown in Fig. 5 provides the opportunity to evaluate several facets of the calculations. To fit the sharp rise near threshold of the (n,2n) cross section accurately, considerable constraint is placed upon the low-energy neutron transmission coefficients as well as the parameters needed to describe competing gamma-ray and charged-particle emission.

Charged-particle production cross sections and spectra resulting from neutron reactions on iron are required for radiation damage calculations and for use in dosimetry applications. An example of the latter data type is the $^{54}$Fe (n,p) cross section to which we compare our calculations in Fig. 6. For this nucleus, proton emission accounts for a significant portion of the total reaction cross section (particularly from this reaction), and the agreement indicates the suitability of the proton optical parameters in a case where competition from neutron emission is small.

New opportunities to evaluate calculated (n,np) and (n,pn) cross sections occur from comparison to recently measured proton-production spectra induced by 15-MeV neutrons [21] as shown in Fig. 7 for $^{56}$Fe. The agreement at the low energy end of the spectrum indicates a correct calculation of the (n,np) contribution while the agreement for higher secondary energies indicates a proper preequilibrium fraction, particularly with regard to the relative number of protons and neutrons emitted.

Measurements of alpha-production cross sections on iron have been relatively few, consisting mainly of several values of the $^{54}$Fe (n,$\alpha$) cross section at 14 MeV. Recently measurements by Paulsen [22] of the $^{54}$Fe (n,$\alpha$) reaction below 10 MeV and by Grimes et al. [21] of 15-MeV neutron-induced alpha production on $^{54,56}$Fe have improved this situation considerably. Our calculations of the $^{54}$Fe (n,$\alpha$) cross section from threshold to 40 MeV are compared to experimental results in Fig. 8. Since total charged-particle production cross sections are needed for radiation damage calculations, we illustrate in Fig. 9 the total production of protons and alphas on $^{54,56}$Fe up to 40 MeV. The arrows indicate thresholds for (n,xnp) and (n,xn$\alpha$) reactions. Comparisons are made to (n,p) or (n,$\alpha$) data occurring below the first arrow and to the 15-MeV total production cross sections now available.

Gamma-ray production data also play an important role in applications such as shielding calculations. To accurately calculate such data, a detailed gamma-ray cascade model was included and all residual nuclei populated by major reactions were allowed to gamma decay. Quite a large amount of data exist up to 20 MeV, both spectral and production cross sections for discrete lines, that allow the calculations to be further verified. Figures 10 and 11 compare calculations to two such data types--(1) gamma-ray production spectra induced by 14-MeV neutrons as measured by Drake [23] and (2)

the excitation function for production of the 1.238 MeV gamma-ray in $^{56}Fe$.

As a supplement to neutron-induced reaction data on iron, we used proton data to provide further checks on parameter sets in energy regions where neutron data are lacking. Figure 12 shows the measured $^{56}Fe$ (p,n) and (p,2n) cross sections [24,25] to which we compare our calculated results. Through such comparisons, the behavior of proton and neutron transmission coefficients, level density parameters, and preequilibrium corrections can be tested at higher incident energies.

Cross sections for major reactions and production spectra for neutron and gamma-ray emission obtained from these calculations were incorporated into an ENDF-like evaluation extending to 40 MeV. Dosimetry files were provided for $^{54,56}Fe$ while a complete evaluation was provided for natural iron. Below 20 MeV, standard formats and representations were used, making this portion compatible with existing processing and other applications codes. Above 20 MeV, new formats had to be devised to accomodate energy-angle correlations as well as to simplify presentation of data for energies where many reaction channels were open.

## REFERENCES


1. W. Hauser and H. Feshbach, Phys. Rev. 87, 336 (1952).

2. I. Zanelli et al., "Measurements of Neutron Total and Non-elastic Cross Sections for C, O, Ca, and Fe," contribution to this Symposium.

3. F. G. Perey, Phys. Rev. 131, 745 (1962).

4. O. F. Lemos, "Diffusion Elastique de Particules Alpha de 21 a 29.6 MeV sur des Noyaux de la Region Ti-Zn," Orsay report, Series A, No. 136 (1972).

5. D. M. Brink, thesis, Oxford University (1955), unpublished; P. Axel, Phys. Rev. 126, 671 (1962).

6. A. Gilbert and A. G. W. Cameron, Can. J. Phys. 43, 1446 (1965).

7. J. L. Cook, H. Ferguson, and A. R. de L. Musgrove, Aust. J. Phys. 20, 447 (1967).

8. C. Kalbach, Z. Phys. A283, 401 (1977).

9. C. Kalbach, Z. Phys. A287, 319 (1978).

10. G. S. Mani, Nucl. Phys. A165, 225 (1977).

11. P. D. Kunz, "DWUCK - A Distorted Wave Born Approximation Program," unpublished.

12. C. L. Dunford, "A Unified Model for Analyses of Compound Nucleus Reactions," AI-AEC-12931, Atomics International (1970).

13. P. G. Young and E. D. Arthur, "GNASH: A Preequilibrium Statistical Model Code for Calculation of Cross Sections and Emission Spectra," LA-6947, Los Alamos Scientific Laboratory (1977).

14. J. L. Kammerdiener, "Neutron Spectra Emitted by $^{239}Pu$, $^{238}U$, $^{235}U$, Pb, Nb, Ni, Fe, Al, and C Irradiated by 14 MeV Neutrons," UCRL-51232, Lawrence Livermore Laboratory (1972).

15. B. E. Leshchenko et al., Sov. J. Nucl. Phys. 15, 5 (1972).

16. M. Hyakutake et al., J. Phys. Soc. Japan 38, 606 (1975).

17. C. Kalbach and F. M. Mann, to be published.

18. D. Hermsdorf et al., "Differentielle Neutronenemissionsquerschitte bei 14.6 MeV Einschussenergie," Dresden report ZFK-277 (1974).

19. J. Frehaut and G. Mosinski, Nuclear Cross Sections and Technology Conference, NBS Special Publication 425 (1975), p. 855.

20. L. R. Veeser, personal communication (1979).

21. S. M. Grimes et al., Phys. Rev. C19, 2127 (1979).

22. A. Paulsen et al., Nucl. Sci. Eng. 72, 113 (1979).

23. D. M. Drake, E. D. Arthur, and M. G. Silbert, Nucl. Sci. Eng. 65, 49 (1978).

24. R. Michel et al., Nucl. Phys. A322, 40 (1979).

25. I. L. Jenkins and A. G. Wain, J. Inorg. Nucl. Chem. 32, 1419 (1970).

TABLE I

Optical Parameters

| | r(fm) | a(fm) |
|---|---|---|
| Neutrons | | |
| $V(MeV) = 49.747 - 0.4295E - 0.0003E^2$ | 1.287 | 0.56 |
| $W_{vol}(MeV) = -0.207 + 0.253E$ | 1.345 | 0.47 |
| $V_{SO}(MeV) = 6.2$ | 1.12 | 0.47 |
| $W_{SD}(MeV) = 6.053 + 0.074E$ | 1.3448 | 0.47 |
| Above 6 MeV | | |
| $W_{SD}(MeV) = 6.497 - 0.325(E-6)$ | | |
| Protons | | |
| $V(MeV) = 58.384 - 0.55E$ | 1.25 | 0.65 |
| $W_{SD}(MeV) = 13.5 - 0.15E$ | 1.25 | 0.47 |
| $V_{SO}(MeV) = 7.5$ | 1.25 | 0.47 |
| $r_c(fm) = 1.25$ | | |
| Alphas | | |
| $V(MeV) = 193 - 0.15E$ | 1.37 | 0.56 |
| $W_{vol}(MeV) = 21 + 0.25E$ | 1.37 | 0.56 |
| $r_c(fm) = 1.4$ | | |

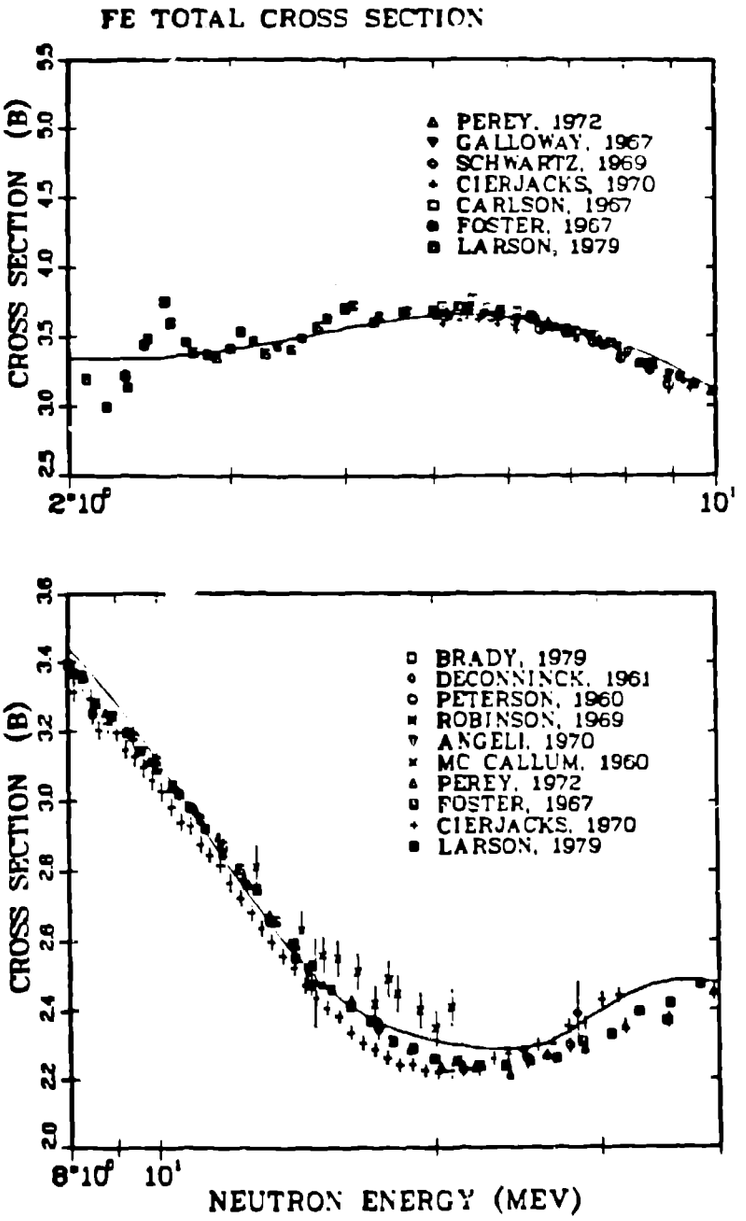


Fig. 1. Total cross-section data and values calculated using the neutron optical parameters of Table I.

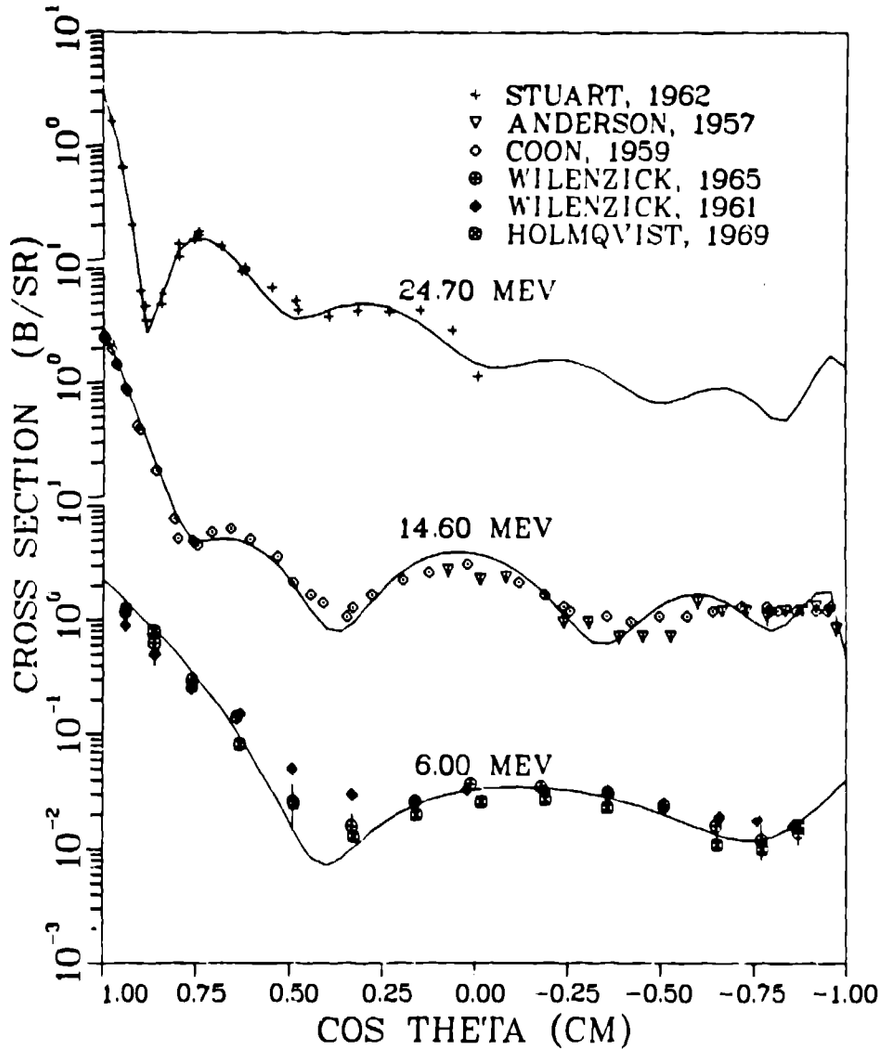


Fig. 2. Experimental and theoretical elastic scattering angular distributions.

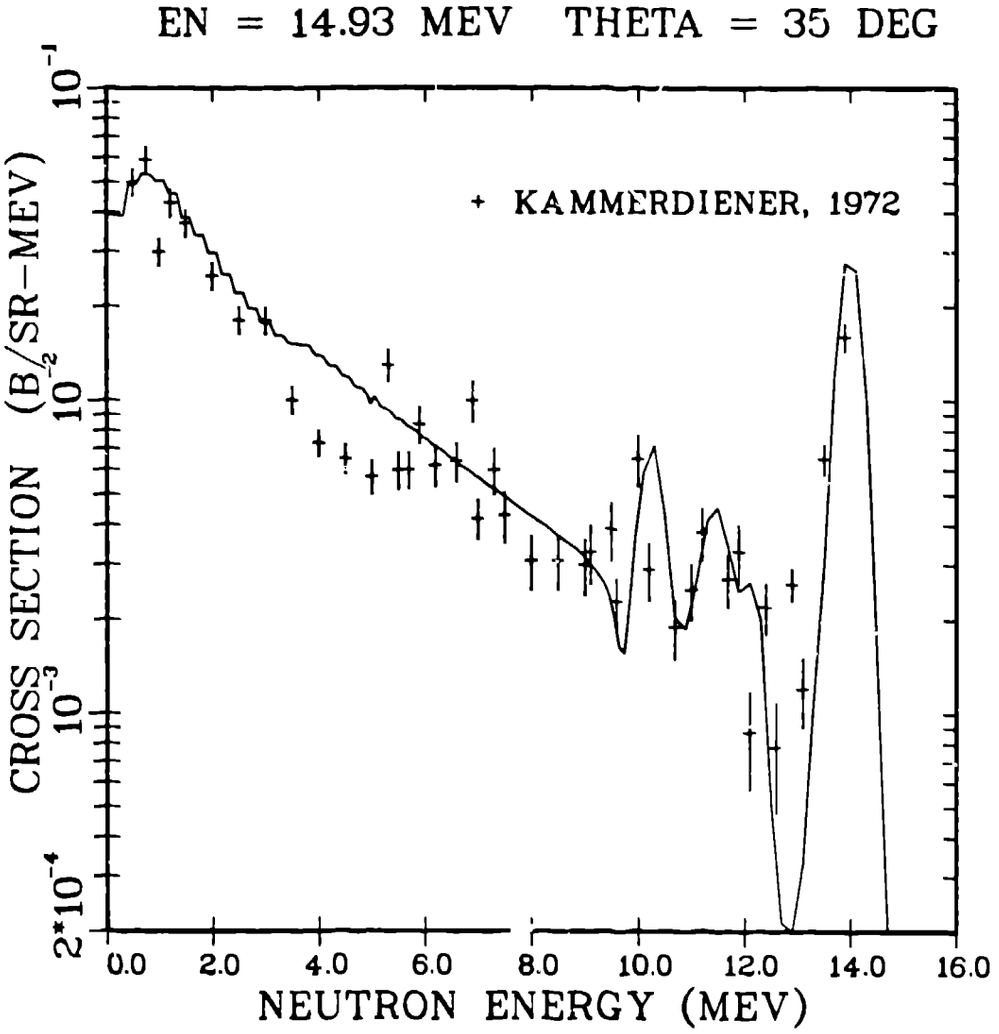


Fig. 3. The calculated neutron emission spectrum induced by 14.9 MeV neutrons is compared to results measured by Kammerdiener.

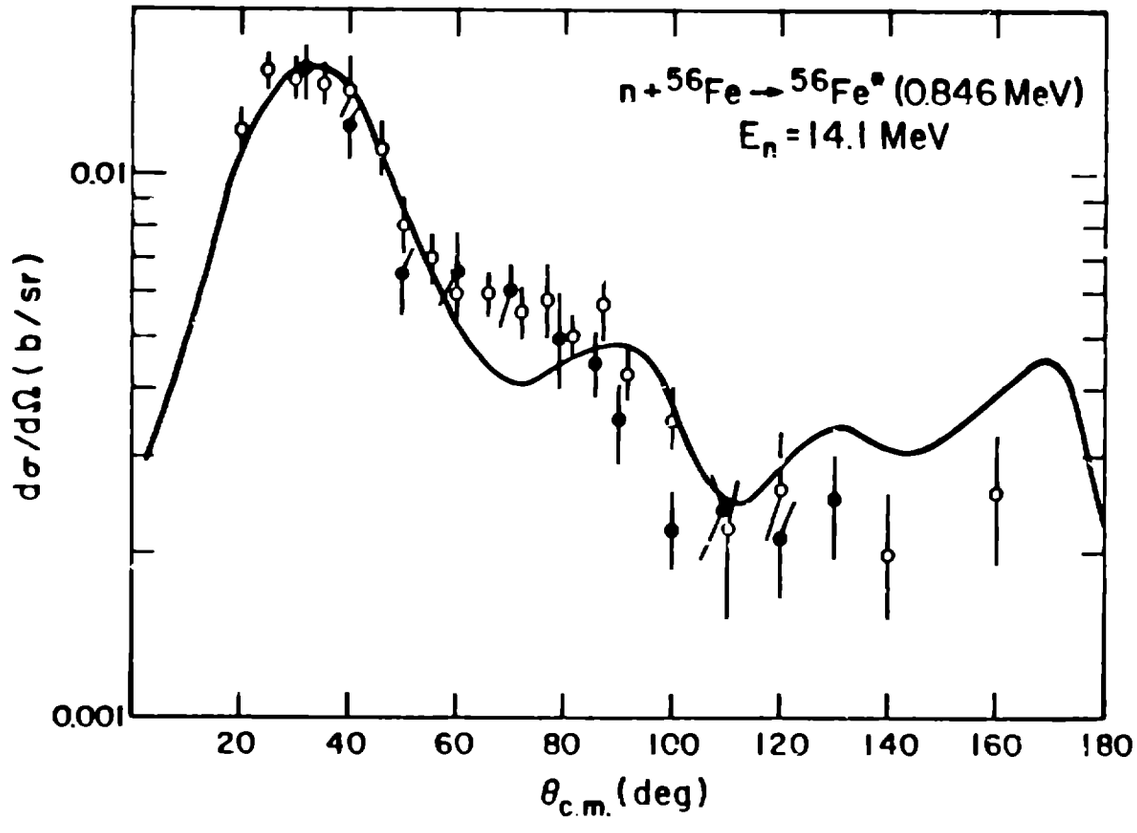


Fig. 4. The theoretical and experimental (closed and open circles are references 15 and 16, respectively) angular distributions for excitation of the 0.846 MeV level in $^{56}Fe$ by 14 MeV neutrons.

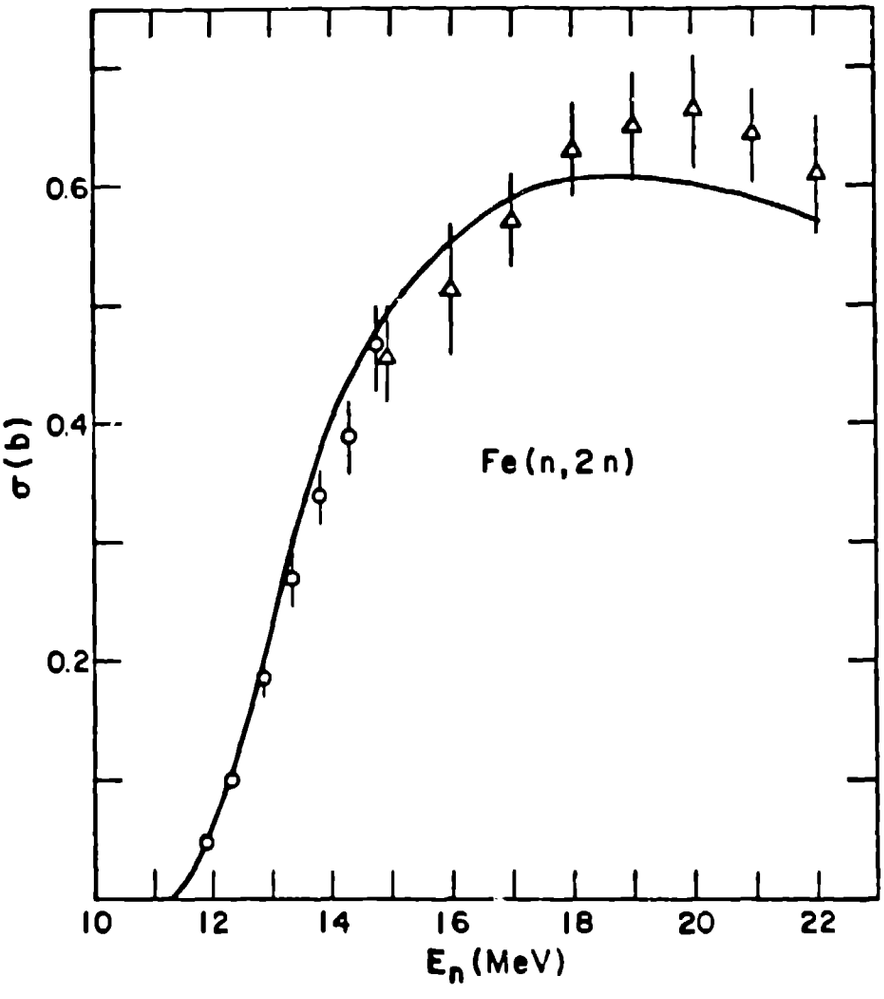


Fig. 5. Calculated and experimental values (circles, Ref. 19; triangles, Ref. 20) for the (n,2n) cross section on natural iron.

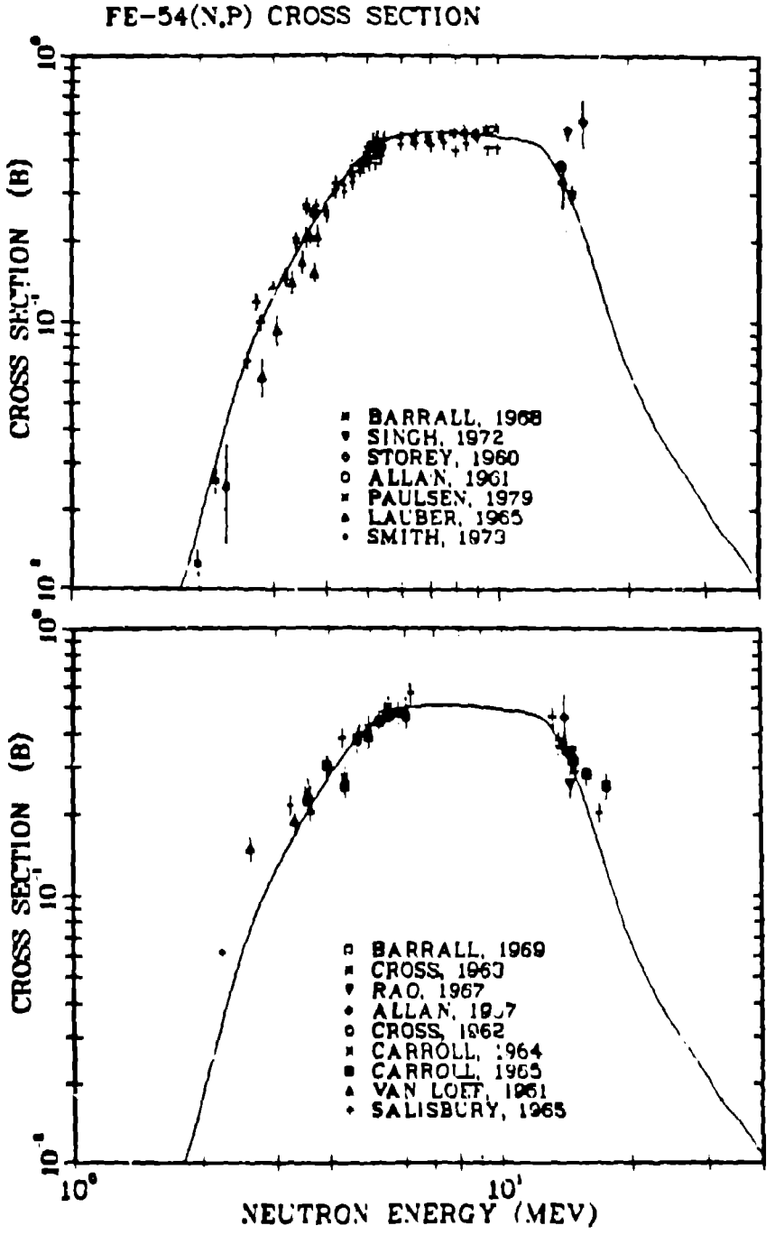


Fig. 6. Theoretical and experimental $^{54}Fe$ (n,p) cross sections.

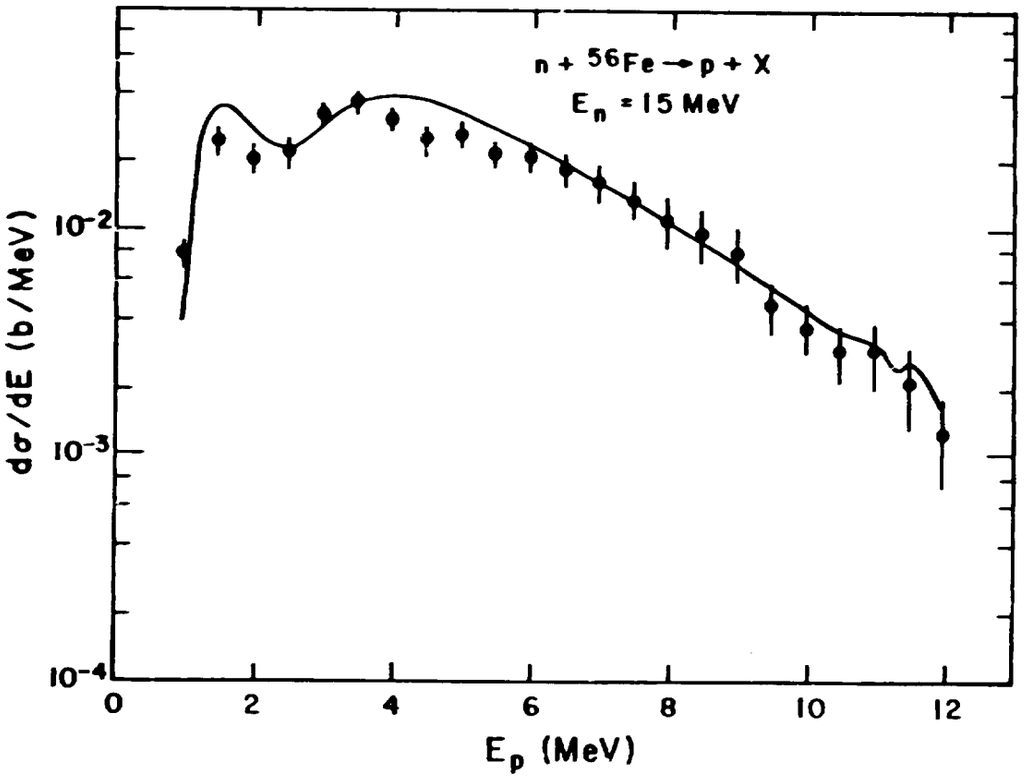


Fig. 7. Calculated values for the proton emission spectrum induced by 15-MeV neutrons on $^{56}Fe$ are compared to the Grimes[21] data.

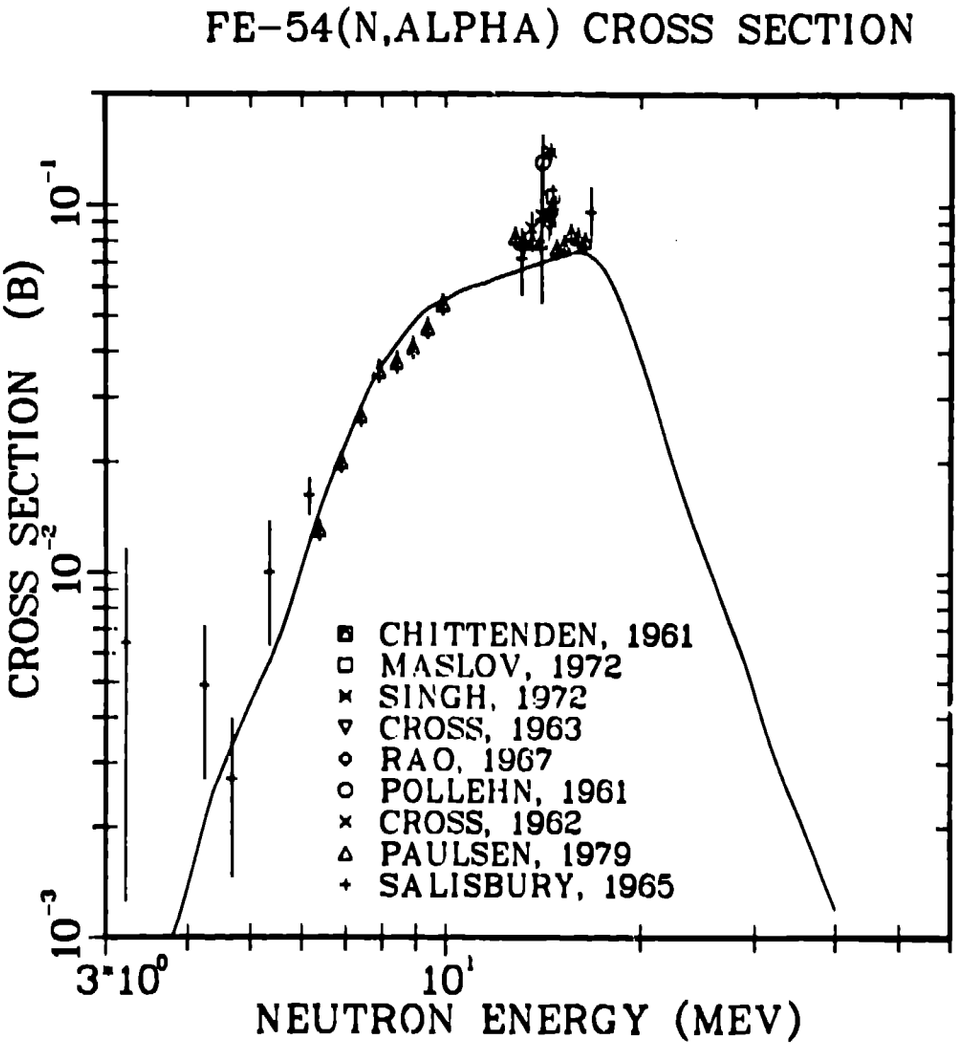


Fig. 8. Theoretical and experimental $^{54}Fe$ (n,α) values between 3 and 40 MeV.

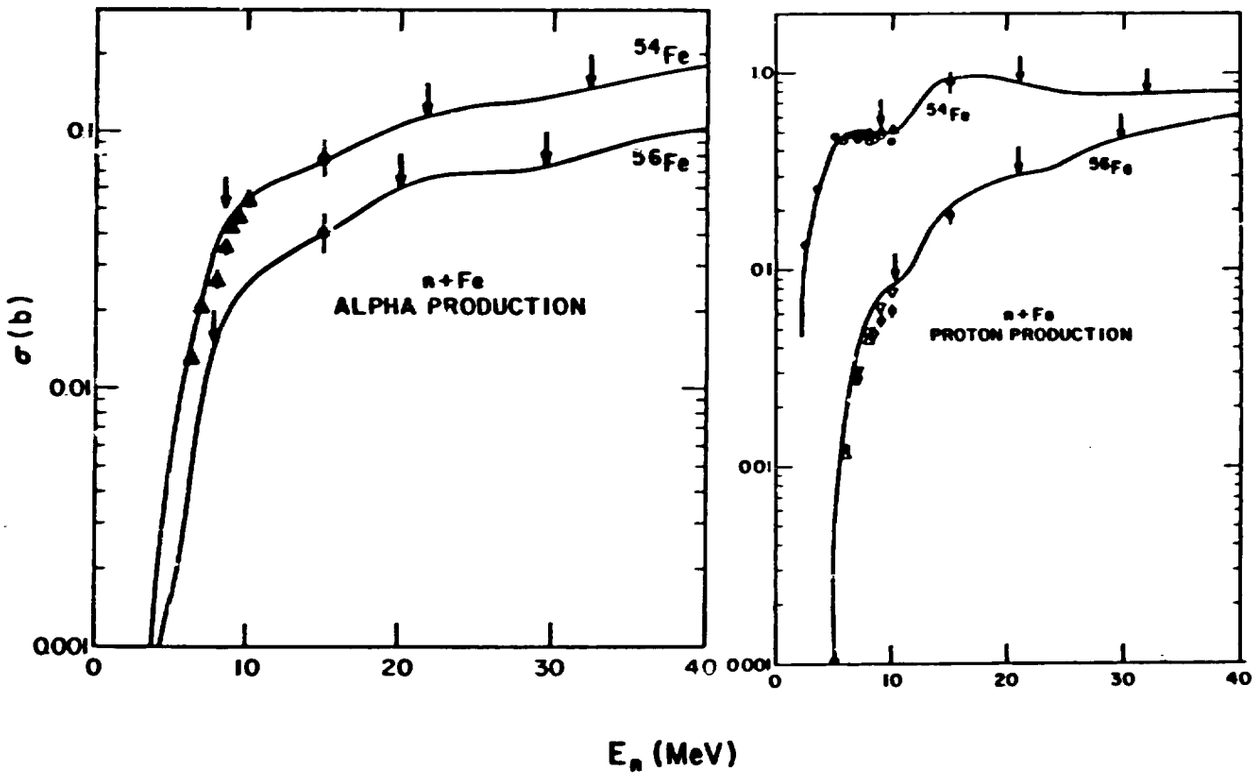


Fig. 9. Total proton- and alpha-production cross sections calculated for $^{54}Fe$ and $^{56}Fe$. The arrows indicate thresholds for (n,xnp) and (n,xn$\alpha$) reactions.

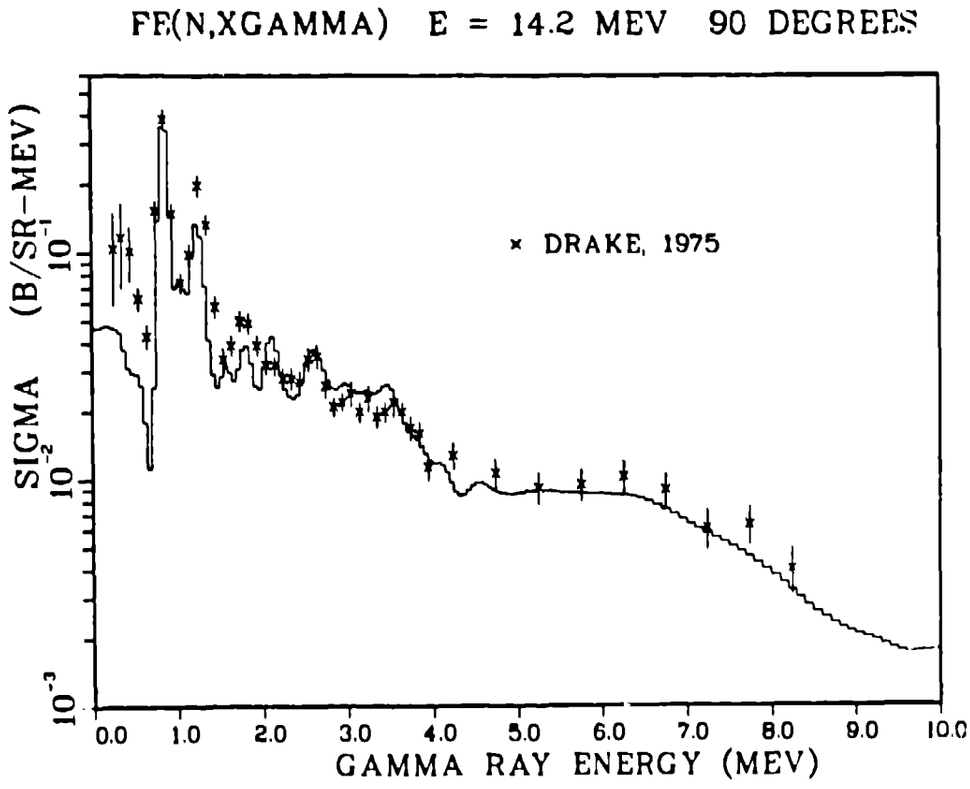


Fig. 10. The calculated gamma-ray production spectrum induced by 14.2 MeV neutrons is compared to data measured by Drake.[23]

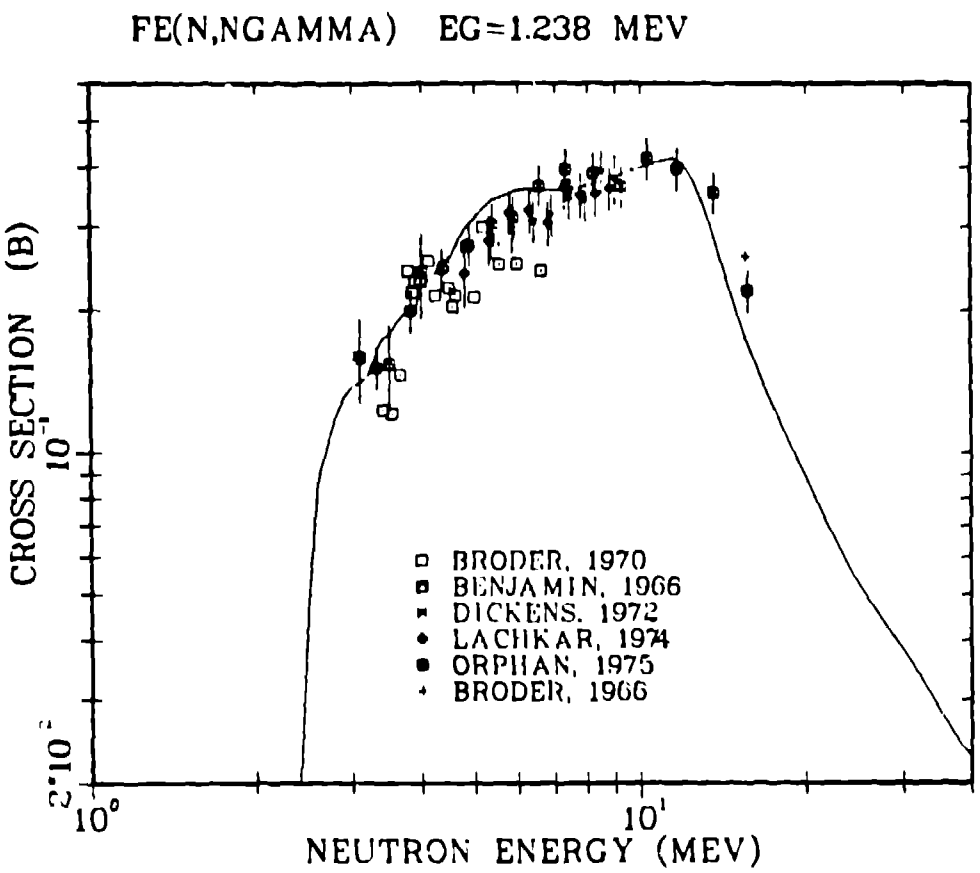


Fig. 11. Theoretical and experimental values for excitation of the 1.238-MeV gamma ray by neutron interactions with iron.

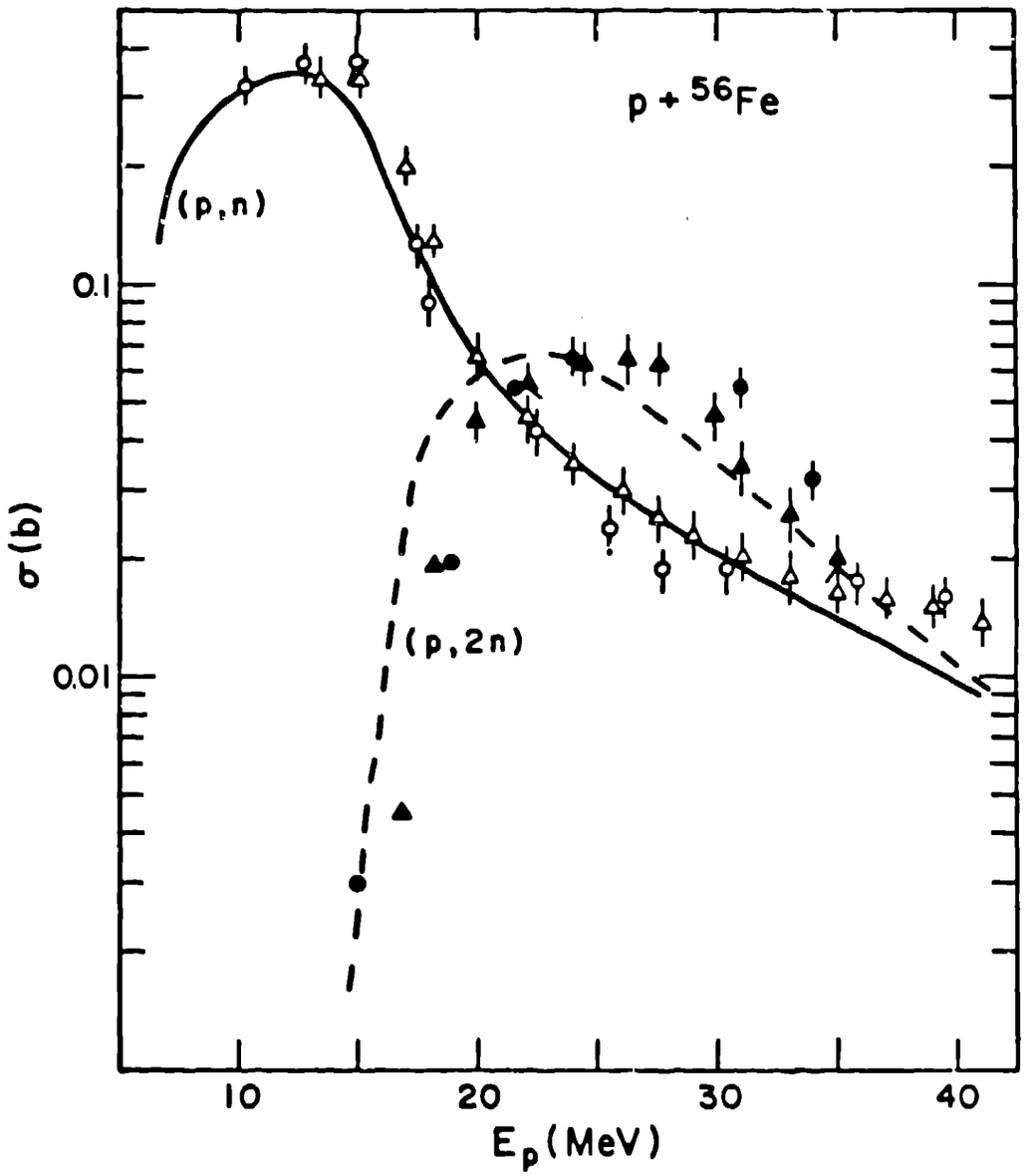


Fig. 12. Calculated and experimental cross sections for $^{56}Fe$ (p,xn) reactions. (Circles are Ref. 24; triangles are Ref. 25.)